*Progress In Electromagnetics Research C, Vol. 95, 1–13, 2019*

# Scattering from a Distribution of Rough Plates

**Max Bright*, Akira Ishimaru, and Yasuo Kuga**

**Abstract**—Modeling how electromagnetic waves scatter from a distribution of rough plates poses many applications. Certain systems may be easy to approximate with planar geometry, but use of numerical field solvers to determine the radiated fields could take a long time for nontrivial structures. We propose a new approach based on the Kirchhoff approximation. This method will consider the case of multiple rough, finite-sized rectangular plates. The solution was used for developing software to determine the scattering of waves off of a distribution of rough plates of arbitrary position and orientation between a transmitter and receiver. The method considers each plate individually, calculating the coherent and incoherent scattered fields. Provided that all plates and the transmitter and receiver are sufficiently spaced, we calculate the total fields by summing the result from each individual plate. For many practical situations, the distance from the plate to the receiver may not be much greater than the size of the plate. We will show that the common far-field approximation of the Green's function is not valid for these cases, and we will have to use a more accurate approximation of Green's function.

## 1. INTRODUCTION

This paper will discuss modeling scattered fields from distributions of objects that can be represented as planar geometry. Such objects include house rooftops, building walls and windows, solar panels, car rooftops, and many other types of geometry of interest in an urban environment. More abstractly, this concerns how to model the radiation characteristic of a distribution of finite size rough rectangular plates. Such a model will be useful for determining interference in communication systems, such as unwanted reflections off of nearby objects. In addition, the problem can be worked backwards. Given a method for calculating the radiated fields, a desired radiation characteristic could be determined, and an algorithm could be implemented to optimize plate locations to achieve the desired pattern.

There are two existing ways to approach this problem. For instance, reflections off of flat plates are well understood [1]. Due to the existence of analytic solutions for the scattered fields, the algorithm can run very quickly; however, there are tradeoffs. For example, surface roughness parameters are not considered. In addition, the edge effects of the plate are neglected. Another possibility is the use of numerical methods. While numerical analysis techniques such as the Finite Element Method can yield very accurate results, there is a significant tradeoff in computation time and efficiency [2, 3].

Scattering from infinite rough surfaces has been extensively studied [4]. The Small Perturbation Method and Kirchhoff Approximation are widely used for such problems, particularly when the surface height variation is quasi-periodic [5]. Another Kirchoff Approximation-based method developed in [6] takes into account known values for surface height variation, such as data pulled from Earth terrain elevation data. However, the method does not account for when the surface height is given by a Gaussian random distribution, as would be the case for minor variations in materials such as soil or pavement.

The study of scattering from finite-size rough surfaces is limited. This paper will introduce an approach for modeling scattering off of plates that will add consideration of roughness effects. Analytic equations will be used, which will yield a significant computational advantage over numerical methods.

*Received 30 April 2019, Accepted 26 July 2019, Scheduled 9 August 2019*
* Corresponding author: Max Bright (mabright@umich.edu).
The authors are with the Electrical Engineering Department, University of Washington, Seattle, WA, USA.

## 2. KIRCHHOFF APPROXIMATION FOR A SINGLE PLATE

### 2.1. Coordinate System and Definitions

We will begin by modeling scattering from a single plate.

Figure 1 shows the coordinate system and definitions that we will use for the TM case. For TE case, we make the substitutions: $\hat{h}_i(+\bar{H})$ becomes $\hat{h}_i(+\bar{E})$, $\hat{v}_i(+\bar{E})$ becomes $\hat{v}_i(-\bar{H})$, $\hat{v}_s(+\bar{E})$ becomes $\hat{v}_s(+\bar{H})$, and $\hat{h}_s(-\bar{H})$ becomes $\hat{h}_s(+\bar{E})$.

We define a plate as a rectangular surface of dimensions $2a \times 2b$. We assume that the plate thickness is much larger than the skin depth. We will consider a transmitter and receiver at arbitrary locations relative to the plate, and we will consider incidence in TM and TE cases, with polarizations defined in terms of $\hat{v}$ and $\hat{h}$ vectors. The coordinate system is outlined in Fig. 1.

A Gaussian model will be used for modeling the roughness of the plate surface. This yields two parameters: the surface root mean square (rms) height $\langle h \rangle$, which indicates the height variance, and

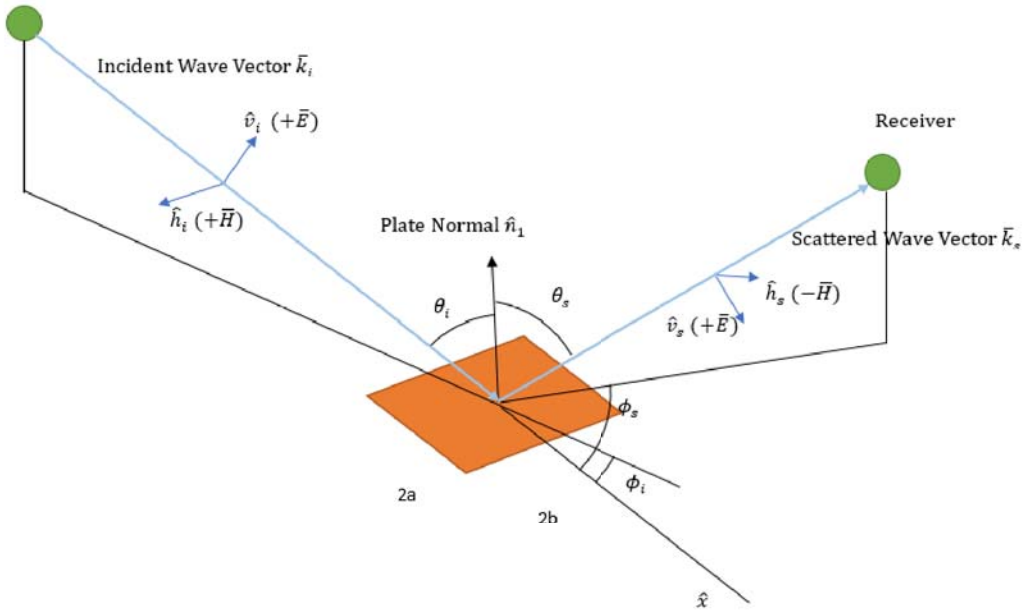


**Figure 1.** Coordinate system for a single plate, TM case.

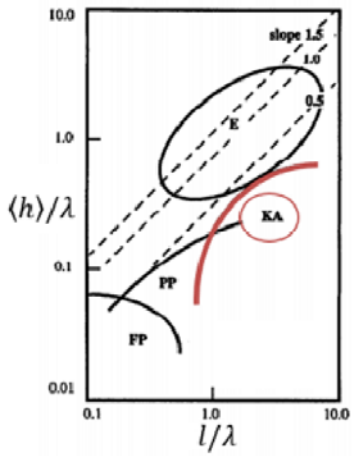


**Figure 2.** Valid region for Kirchhoff approximation in terms of surface roughness [7].

the correlation length $l$, which indicates the distance between similar features in the surface. Both contribute to the surface slope, and the Kirchhoff approximation is valid for certain surface slope cases which can be seen in Fig. 2 [7].

We want to derive scattering amplitudes, which let us relate coherent incident and scattered electric fields, and the cross sections, which let us evaluate incoherent scattered power.

### 2.2. Equation Setup

We begin with the basic assumption of the Kirchhoff approximation, requiring that the fields locally reflected on the plate are equal to the incident fields [2–4]. We start with

$$\begin{aligned} \hat{n}_1 \times \bar{H}_r &= \hat{n}_1 \times \bar{H}_{surf} \\ \bar{E}_r \times \hat{n}_1 &= \bar{E}_{surf} \times \hat{n}_1 \end{aligned} \tag{1}$$

where we define $\bar{H}_r$ and $\bar{E}_r$ as the reflected $E$ and $H$ fields in specular directions, and

$$|E_{surf}| = R_{\perp/\|} \, |E_i| \, e^{-ik_i \cdot \bar{r}_1} \tag{2}$$

where $R_{\perp/\|}$ is the infinite flat surface reflection coefficient, in either parallel ($R_\|$) or perpendicular ($R_\perp$) polarization. We will denote:

$$\bar{E}_{is} = \frac{\bar{E}_{surf}}{e^{-ik_i \cdot \bar{r}_1}} \tag{3}$$

Similar definitions follow for $\bar{H}$.

From the Franz equations, following the derivation in [8], we have:

$$\bar{E} = \nabla \times \nabla \times \bar{\Pi} + i\omega\mu \nabla \times \bar{\Pi}_m \tag{4}$$

Where

$$\begin{aligned} \bar{\Pi} &= \frac{1}{i\omega\epsilon} \int_S \hat{n} \times \bar{H}_i G dx dy \\ \bar{\Pi}_m &= \frac{1}{i\omega\mu} \int_S \bar{E}_i \times \hat{n} G dx dy \end{aligned} \tag{5}$$

and $G$ is the free space Green's function:

$$G = \frac{e^{ik|\bar{r} - \bar{r}_1|}}{4\pi \, |\bar{r} - \bar{r}_1|} \tag{6}$$

And $S$ is the plate surface: $-a < x < a$, $-b < y < b$.

### 2.3. Green's Function Approximation

For the scattering problem, a far field approximation is commonly used for Green's function. However, we will show that a simple far field approximation is not valid for scattering from a finite size plate in some cases. Therefore, we want to simplify Eq. (6) by performing a Taylor expansion on the argument of the exponential and keeping an extra term:

$$ik \, |\bar{r} - \bar{r}_1|$$

which is equivalently

$$ik\sqrt{R_0^2 + \vec{r}_1^2 - 2R_0 \vec{r}_1 \cdot \hat{k}_s} = ikR_0\sqrt{1 - X}$$

where $R_0$ is the distance from the center of the plate to the receiver

$$X = \frac{2R_0 \vec{r}_1 \cdot \hat{k}_s - |\vec{r}_1|^2}{R_0^2} \tag{7}$$

We know the first order Taylor expansion for a square root is:

$$\sqrt{1 - X} \cong 1 - \frac{1}{2}X$$

So

$$ikR_0\sqrt{1-X} = ikR_0\left(1-\frac{1}{2}\left(\frac{2R_0\vec{r}_1\cdot\hat{k}_s-\left|\vec{r}_1\right|^2}{R_0^2}\right)\right)$$

Therefore

$$ik\left|\bar{r}-\bar{r}_1\right| \cong ik\left[R_0-\vec{r}_1\cdot\hat{k}_s+\frac{\left|\vec{r}_1\right|^2}{2R_0}\right] \tag{8}$$

So $G$ can now be approximated as:

$$G \cong \frac{e^{ikR_0-i\left(\bar{k}_s\right)\cdot\bar{r}_1+\frac{ik\left(x^2+y^2\right)}{2R_0}}}{4\pi R_0} \tag{9}$$

The normal far field approximation would have only used the first two terms in Eq. (7):

$$G \cong \frac{e^{ikR_0-i\left(\bar{k}_s\right)\cdot\bar{r}_1}}{4\pi R_0} \tag{10}$$

### 2.4. $\mathbf{E_i}$ and $\mathbf{E_s}$ Relationships

In the far field, $\bar{k}_s$ is proportional to $e^{i\left(\bar{k}_s\right)\cdot\bar{r}_1}$. We have

$$\nabla e^{i\left(\bar{k}_s\right)\cdot\bar{r}_1} = i(\bar{k}_s)\cdot e^{i\left(\bar{k}_s\right)\cdot\bar{r}_1}$$

Therefore, an operation $\nabla$ is equivalent to $i(\bar{k}_s)$. This means:

$$\begin{aligned}\nabla\times\nabla\times\ldots &= -k^2\left(\hat{k}_s\right)\times\left(\hat{k}_s\right)\times\ldots\\ \nabla\times\ldots &= i\left(\bar{k}_s\right)\times\ldots\end{aligned} \tag{11}$$

Therefore:

$$\begin{aligned}E_{sv} \;=\; &\frac{i\omega\mu}{4\pi R_0}e^{ikR_0}\int_S\hat{v}\cdot\left(\hat{n}\times\bar{H}_{surf}\right)e^{-i\left(\bar{k}_s\right)\cdot\bar{r}_1}e^{\frac{ik\left(x^2+y^2\right)}{2R_0}}dxdy\\ &-\frac{ik}{4\pi R_0}e^{ikR_0}\int_S\hat{h}\cdot\left(\bar{E}_{surf}\times\hat{n}\right)e^{i\left(\bar{k}_s\right)\cdot\bar{r}_1}e^{\frac{ik\left(x^2+y^2\right)}{2R_0}}dxdy\end{aligned} \tag{12}$$

For $\bar{E}_{sh}$, vector $\hat{v}$ is replaced by $\hat{h}$, and $\hat{h}$ is replaced by $\hat{v}$.

Splitting $\bar{E}_i$ into $v$ and $h$ components (TM and TE), we get:

$$\begin{bmatrix}E_{sv}\\E_{sh}\end{bmatrix} = \tfrac{1}{R_0}e^{ikR_0}\begin{bmatrix}f_{vv} & f_{vh}\\ f_{hv} & f_{hh}\end{bmatrix}\begin{bmatrix}E_{iv}\\E_{ih}\end{bmatrix} \tag{13}$$

where:

$$\begin{aligned}E_{iv}f_{vv} &= \frac{ik}{4\pi}\left(\hat{v}_s\cdot\left(\hat{n}\times\frac{\omega\mu}{k}\bar{H}_{is}\right)_{TM}-\hat{h}_s\cdot\left(\bar{E}_{is}\times\hat{n}\right)_{TM}\right)I\\ E_{ih}f_{vh} &= \frac{ik}{4\pi}\left(\hat{v}_s\cdot\left(\hat{n}\times\frac{\omega\mu}{k}\bar{H}_{is}\right)_{TE}-\hat{h}_s\cdot\left(\bar{E}_{is}\times\hat{n}\right)_{TE}\right)I\\ E_{iv}f_{hv} &= \frac{ik}{4\pi}\left(-\hat{h}_s\cdot\left(\hat{n}\times\frac{\omega\mu}{k}\bar{H}_{is}\right)_{TM}-\hat{v}_s\cdot\left(\bar{E}_{is}\times\hat{n}\right)_{TM}\right)I\\ E_{ih}f_{hh} &= \frac{ik}{4\pi}\left(-\hat{h}_s\cdot\left(\hat{n}\times\frac{\omega\mu}{k}\bar{H}_{is}\right)_{TE}-\hat{v}_s\cdot\left(\bar{E}_{is}\times\hat{n}\right)_{TE}\right)I\end{aligned} \tag{14}$$

$$I = \int_s e^{i\left(\bar{k}_s-\bar{k}_i\right)\cdot\bar{r}_1}e^{\frac{ik\left(x^2+y^2\right)}{2R_0}}dS \tag{15}$$

Although we are using $I$ in Eq. (15), $I$ is not the intensity of the field.

### 2.5. Evaluation of I

Evaluation of $\int e^{i\left(\bar{K}-\bar{K_i}\right)\cdot\bar{r_1}}dS$:

$$\bar{r}_1 = \begin{bmatrix} x \\ y \\ f(x,y) \end{bmatrix}$$

So the integral is equivalently:

$$I = \int\limits_S e^{-i\bar{v}\cdot\bar{r_1}} e^{-iv_z f(x,y)} e^{\frac{ik\left(x^2+y^2\right)}{2R_0}} dS \tag{16}$$

where we define:

$$\bar{v} = \begin{bmatrix} k_{s_x} - k_{i_x} \\ k_{s_y} - k_{i_y} \\ 0 \end{bmatrix} = \begin{bmatrix} k_x \\ k_y \\ 0 \end{bmatrix}$$

$$v_z = k_{s_z} - k_{i_z} = k(\cos(\theta_s) + \cos(\theta_i))$$

Since we cannot evaluate the surface height $f(xy)$ directly, we evaluate (16) as an average:

$$\langle I\rangle = \int\limits_S e^{-i\bar{v}\cdot\bar{r_1}} \left\langle e^{-iv_z f(x,y)} \right\rangle e^{\frac{ik\left(x^2+y^2\right)}{2R_0}} dxdy$$

where we can find

$$\left\langle e^{-iv_z f(x,y)} \right\rangle = e^{-\frac{1}{2}v_z^2\langle h\rangle^2} \tag{17}$$

where $\langle h\rangle$ is the surface rms height.

Rearranging, we get:

$$\langle I\rangle = e^{-\frac{1}{2}v_z^2\langle h\rangle^2} \left( \int\limits_{-a}^{a} e^{-ik_x * x} e^{\frac{ik}{2R_0}\left(x^2\right)} dx \right) \left( \int\limits_{-b}^{b} e^{-ik_y * y} e^{\frac{ik}{2R_0}\left(y^2\right)} dy \right)$$

Evaluating the integral, we get:

$$\langle I\rangle = \hat{I}\left(k_x, a\right) \hat{I}\left(k_y, b\right) e^{-\frac{1}{2}k^2(\cos(\theta_s)+\cos(\theta_i))^2\langle h\rangle^2} \tag{18}$$

where

$$\hat{I}\left(k_n, c\right) = \frac{(-1)^{\frac{1}{4}} e^{-\frac{ik_n^2 R_0}{2k}} \sqrt{\pi}}{\sqrt{\frac{2k}{R_0}}} \left( \mathrm{Erf}\left( \frac{(-1)^{\frac{3}{4}} \left( -c\frac{k}{R_0} + k_n \right)}{\sqrt{\frac{2k}{R_0}}} \right) - \mathrm{Erf}\left( \frac{(-1)^{\frac{3}{4}} \left( 2c\frac{k}{R_0} + k_n \right)}{\sqrt{\frac{2k}{R_0}}} \right) \right)$$

where $k_n$ corresponds to either $k_x$ or $k_y$, and $c$ corresponds to either $a$ or $b$

If we used the simple far field approximation given by Eq. (10), we would have gotten

$$\langle I\rangle = (2a)(2b) I_x I_y e^{-\frac{1}{2}k^2(\cos(\theta_s)+\cos(\theta_i))^2\langle h\rangle^2} \tag{19}$$

where

$$I_x = \frac{\sin(k_x a)}{k_x a}, \quad I_y = \frac{\sin(k_x b)}{k_y b}$$

Later we will show that the error in $\langle I\rangle$ becomes unacceptable if we use Eq. (19)

### 2.6. Evaluation of Scattering Amplitudes f

Continuing from Eq. (14) we can calculate the locally reflected surface fields as:

$$\left(\bar{H}_{is}\right)_{TM} = -R_{\parallel} H_i \hat{h}_r \quad \left(\bar{H}_{is}\right)_{TE} = R_{\perp} H_i \hat{v_r}$$
$$\left(\bar{E}_{is}\right)_{TM} = R_{\parallel} E_i \hat{v_r} \quad \left(\bar{E}_{is}\right)_{TE} = R_{\perp} E_i \hat{h}_r$$

where $\hat{h}_r$ and $\hat{v}_r$ are evaluated in the specular direction, and we use the infinite flat surface reflection coefficients $R_{\parallel}$ and $R_{\perp}$, and $\epsilon_{r0}$ and $\epsilon_{r1}$ are the complex permittivities of the surrounding air and plate, respectively.

Given these and since $|H_i| = \frac{k}{\omega 0 \mu} |E_i|$, we simplify the scattering amplitudes as:

$$\begin{aligned}
f_{vv} &= \frac{ik}{4\pi} R_{\parallel} \left( -\hat{v}_s \cdot \left( \hat{n} \times \hat{h}_r \right) - \hat{h}_s \cdot \left( \hat{v}_r \times \hat{n} \right) \right) I \\
f_{vh} &= \frac{ik}{4\pi} R_{\perp} \left( \hat{v}_s \cdot \left( \hat{n} \times v_r \right) - \hat{h}_s \cdot \left( \hat{h}_r \times \hat{n} \right) \right) I \\
f_{hv} &= \frac{ik}{4\pi} R_{\parallel} \left( \hat{h}_s \cdot \left( \hat{n} \times \hat{h}_r \right) - \hat{v}_s \cdot \left( \hat{v}_r \times \hat{n} \right) \right) I \\
f_{hh} &= \frac{ik}{4\pi} R_{\perp} \left( -\hat{h}_s \cdot \left( \hat{n} \times \hat{v}_r \right) - \hat{v}_s \cdot \left( \hat{h}_r \times \hat{n} \right) \right) I
\end{aligned}$$

Evaluating these in terms of the incident and scattered angles, we arrive at our final expression for the scattering amplitudes:

$$\begin{aligned}
f_{vv} &= \frac{ik}{4\pi} R_{\parallel} I \cos\left(\phi_i - \phi_s\right) \left(\cos\theta_i + \cos\theta_s\right), \quad f_{vh} = -\frac{ik}{4\pi} R_{\perp} I \sin\left(\phi_i - \phi_s\right) \left(1 + \cos\left(\theta_i\right) \cos\left(\theta_s\right)\right) \\
f_{hv} &= -\frac{ik}{4\pi} R_{\parallel} I \sin\left(\phi_i - \phi_s\right) \left(1 + \cos\theta_i \cos\theta_s\right), \quad f_{hh} = \frac{ik}{4\pi} R_{\perp} I \cos\left(\phi_i - \phi_s\right) \left(\cos\theta_i + \cos\theta_s\right)
\end{aligned} \tag{20}$$

### 2.7. Evaluation of Cross Sections $\boldsymbol{\sigma}$

We define the cross sections as:

$$\sigma_{nm} = 4\pi R_0^2 \left\langle \left| \frac{1}{R_0} e^{ikR_0} f_{nm} \right| \right\rangle \tag{21}$$

We also rewrite the scattering amplitudes as:

$$f_{nm} = \pm \frac{ik}{4\pi} R_{\parallel/\perp} A_{nm} I$$

where $A_{nm}$ denotes the trigonometric functions in the scattering amplitudes.

Evaluating this:

$$\left| \frac{1}{R_0} e^{ikR_0} f_{nm} \right|^2 = \frac{k^2}{\left(4\pi R_0\right)^2} \left|A_{nm}\right|^2 R_{\parallel/\perp}^2 \left(I^1\right)^2 \tag{22}$$

We can easily obtain expressions for $\left|A_{nm}\right|^2 R_{\parallel/\perp}^2$. We split the evaluation of $\langle I \rangle$ into coherent and incoherent components. The coherent component was already evaluated for the scattering amplitudes in Eq. (18).

The summation of the coherent and incoherent component is defined to be $I^1 = \langle \langle I I^* \rangle - \langle I \rangle \langle I^* \rangle \rangle$

We start with the definition of our integral again, ignoring the exponential phase term for simplicity:

$$\langle I \rangle = \int_S e^{-i\bar{v} \cdot \bar{r_1}} \langle e^{-iv_z f(x,y)} \rangle dS \tag{23}$$

We begin by considering $I^1 = \langle I I^* \rangle$. We neglect the phase term in the Green's function expansion by using Eq. (10) instead of Eq. (9), to simplify our calculations.

$$I^1 = \int_{S'} \int_S e^{-i\bar{v} \cdot (\bar{r_1} - \bar{r_1}')} \left\langle e^{-iv_z f(x,y) + iv_z f'(x',y')} \right\rangle dS dS'$$

Since $f$ and $f'$ are Gaussian variables, under a first order approximation (assuming high roughness) we get:

$$\left\langle e^{-iv_z f(x,y)+iv_z f'(x',y')} \right\rangle = \exp\left(-\frac{v_z^2\langle h\rangle^2 \left|\bar{r_1}-\bar{r_1}'\right|^2}{l^2}\right) \tag{24}$$

Therefore, the integral evaluates to:

$$I^1 = \frac{(2a)\,(2b)\,\pi l^2}{v_z^2\langle h\rangle^2}\exp\left(-\frac{\left|\bar{k}_s-\bar{k}_i\right|^2 l^2}{4v_z^2\langle h\rangle^2}\right) \tag{25}$$

Therefore, considering the coherent and incoherent cross section components separately, we get:

$$\begin{aligned} \sigma_{coh_{vv}} &= \frac{k^2}{4\pi}\left|A_{vv}\right|^2 R_{\|}^2 I^2 \quad \sigma_{coh_{vh}} = \frac{k^2}{4\pi}\left|A_{vh}\right|^2 R_{\perp}^2 I^2 \\ \sigma_{coh_{hv}} &= \frac{k^2}{4\pi}\left|A_{hv}\right|^2 R_{\|}^2 I^2 \quad \sigma_{coh_{hh}} = \frac{k^2}{4\pi}\left|A_{hh}\right|^2 R_{\perp}^2 I^2 \end{aligned} \tag{26}$$

Incoherent Cross Sections:

$$\begin{aligned} \sigma_{incoh_{vv}} &= \frac{k^2}{4\pi}\left|A_{vv}\right|^2 R_{\|}^2\,(2a)\,(2b)\,\frac{\pi l^2}{v_z^2\langle h\rangle^2}e^{-\frac{\left|\bar{k}_s-\bar{k}_i\right|^2 l^2}{4v_z^2\langle h\rangle^2}} \\ \sigma_{incoh_{vh}} &= \frac{k^2}{4\pi}\left|A_{vh}\right|^2 R_{\perp}^2\,(2a)\,(2b)\,\frac{\pi l^2}{v_z^2\langle h\rangle^2}e^{-\frac{\left|\bar{k}_s-\bar{k}_i\right|^2 l^2}{4v_z^2\langle h\rangle^2}} \\ \sigma_{incoh_{hv}} &= \frac{k^2}{4\pi}\left|A_{hv}\right|^2 R_{\|}^2\,(2a)\,(2b)\,\frac{\pi l^2}{v_z^2\langle h\rangle^2}e^{-\frac{\left|\bar{k}_s-\bar{k}_i\right|^2 l^2}{4v_z^2\langle h\rangle^2}} \\ \sigma_{incoh_{hh}} &= \frac{k^2}{4\pi}\left|A_{hh}\right|^2 R_{\perp}^2\,(2a)\,(2b)\,\frac{\pi l^2}{v_z^2\langle h\rangle^2}e^{-\frac{\left|\bar{k}_s-\bar{k}_i\right|^2 l^2}{4v_z^2\langle h\rangle^2}} \end{aligned} \tag{27}$$

where:

$$v_z = k(\cos(\theta_s)+\cos(\theta_i))$$

Now that we have the cross sections, we can find an expression for the incoherent scattered power:

$$\begin{bmatrix}\langle E_{sv}\rangle^2 \\ \langle E_{sh}\rangle^2\end{bmatrix} = \frac{1}{R_0^2}\begin{bmatrix}\sigma_{incoh_{vv}} & \sigma_{incoh_{vh}} \\ \sigma_{incoh_{hv}} & \sigma_{incoh_{hh}}\end{bmatrix}\begin{bmatrix}\langle E_{iv}\rangle^2 \\ \langle E_{ih}\rangle^2\end{bmatrix} \tag{28}$$

We can now find the complete scattered field by summing the coherent and incoherent values. The Mueller matrix representation, which is a $4\times 4$ matrix, is often used for describing the scattered intensity [2, 4]. Because we expect the correlation between $v$- and $h$-polarizations to be small in our case, the $2\times 2$ matrix given in Eq. (28) will be sufficient.

If the plate has an arbitrary orientation, we can find the incident and scattered vectors and angles via a Euler angle coordinate transformation, using $Z$-$Y'$-$Z''$ format [9].

## 3. MULTIPLE PLATES

The equations here can easily be used to consider scattering off of multiple plates. By linearity, we can simply sum together the fields calculated from each plate considered in isolation. We will once again consider a transmitter and receiver at an arbitrary position relative to a set of plates, each with arbitrary location and orientation. We then iterate through each plate: for each plate, we will repeat our Kirchhoff approximation calculation from the previous section. Coordinate transformations will be used to account for the arbitrary location and orientation of the plate. We will find the scattered coherent fields $E_{sv}E_{sh}$ and the incoherent scattered fields $\langle E_{sv}\rangle$, $\langle E_{sh}\rangle$. Once the values of these are obtained from each plate, the coherent and incoherent fields are all summed together.

## 4. RESULTS AND DISCUSSION

### 4.1. Scattering Amplitudes and Cross Sections

Figures 3–6 show the basic properties of the scattering amplitudes and cross sections. Fig. 3 shows the scattering amplitudes. The summation of the coherent and incoherent cross sections is visualized in Fig. 4. In addition, the correlation length and root mean square height are varied in Figs. 5 and 6. In all three cases, a wave at $\frac{\pi}{4}$ incidence to a $10\lambda \times 10\lambda$ plate was considered. $\phi_i = \phi_s = 0$, and the

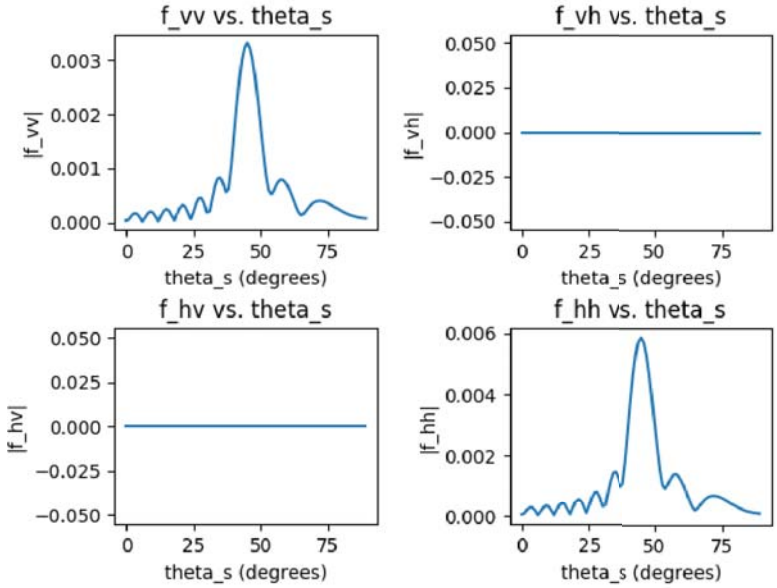


**Figure 3.** Scattering amplitudes $[f]$ versus scattering angle ($f = 28\,\mathrm{GHz}$, $\epsilon_r = 7 + i0.35$, $\theta_i = \frac{\pi}{4}$, $\phi_i = 0$, $\phi_s = 0$, $a = b = 5\lambda$, $\langle h \rangle = 0.1\lambda$, $l = 2\lambda$, $R_0 = 15\lambda$).

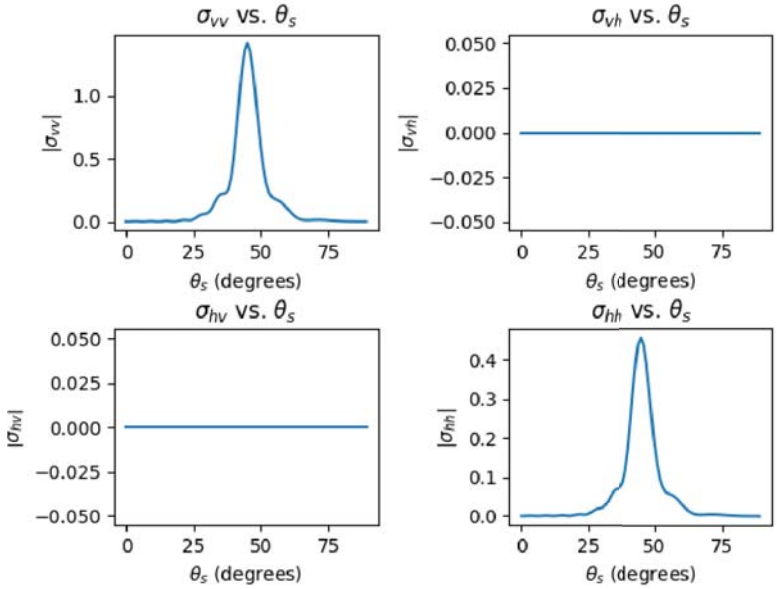


**Figure 4.** Cross sections $[\sigma]$ versus scattering angle ($f = 28\,\mathrm{GHz}$, $\epsilon_r = 7 + i0.35$, $\theta_i = \frac{\pi}{4}$, $\phi_i = 0$, $\phi_s = 0$, $a = b = 5\lambda$, $\langle h \rangle = 0.1\lambda$, $l = 2\lambda$).

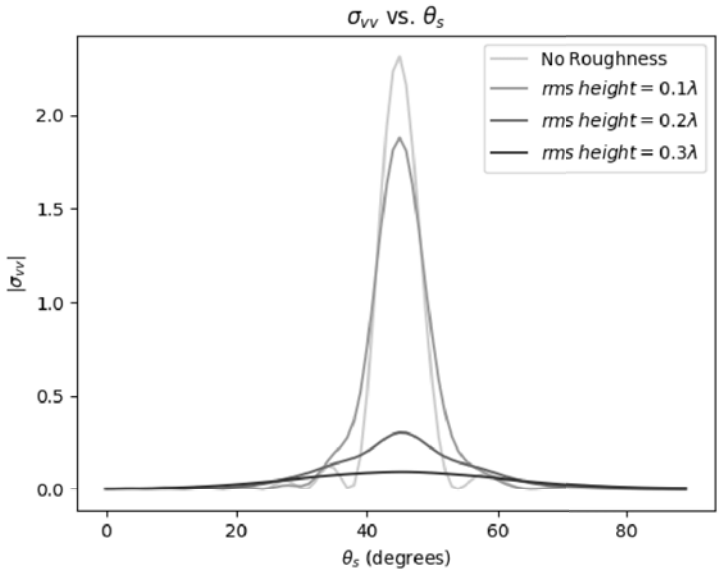


**Figure 5.** Cross section $\sigma_{vv}$ versus scattering angle, for different values of the rms height ($f = 28\,\text{GHz}$, $\epsilon_r = 7 + i0.35$, $\theta_i = \frac{\pi}{4}$, $\phi_i = 0$, $\phi_s = 0$, $a = b = 5\lambda$, $l = 2\lambda$).

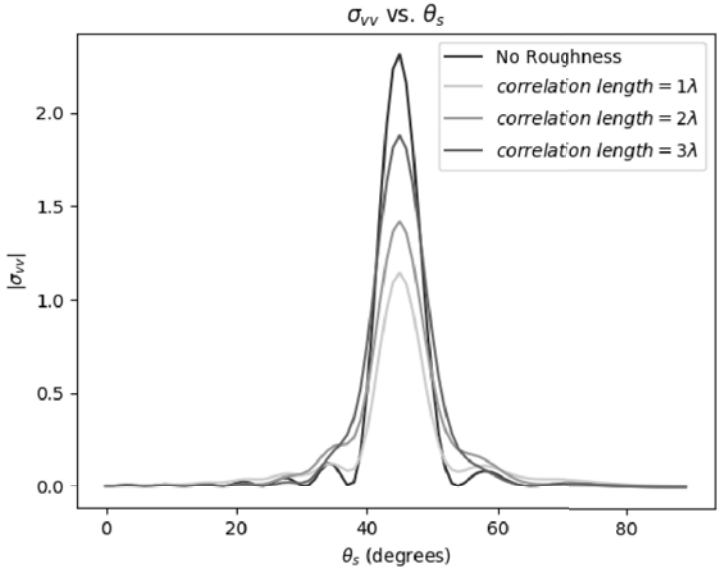


**Figure 6.** Cross section $\sigma_{vv}$ versus scattering angle, for different values of the correlation length ($f = 28\,\text{GHz}$, $\epsilon_r = 7 + i0.35$, $\theta_i = \frac{\pi}{4}$, $\phi_i = 0$, $\phi_s = 0$, $a = b = 5\lambda$, $\langle h \rangle = 0.1\lambda$).

scattered angle $\theta_s$ was swept from 0 to $\frac{\pi}{2}$.

As observed in Figs. 3 and 4, the scattering amplitudes and cross sections exhibit sinc-like behavior. The peak is in the specular direction, which is expected for simple plate geometry. Figs. 5 and 6 show the effects of surface roughness on the cross sections. As seen, when surface roughness is increased, the coherent fields are attenuated. For high roughness, due to most energy being scattered in random directions, the coherent field is almost entirely absent, leaving only a small diffuse component representing the incoherent scattered fields.

We also want to analyze how well our simplified Green's function in Eq. (9) works. Fig. 7 visualizes the effects of the plate area on $f_{vv}$ for different methods of evaluating Green's function.

Our representation of the scattering amplitudes $f_{nm}$ uses the "Improved approximation with phase" evaluation technique, which is a full first-order Taylor expansion, given by Eq. (9). Our formulas for the cross sections $\sigma_{nm}$ use the "Far-field approximation" model, where we perform a first-order Taylor expansion but neglect the phase term, using $\langle I \rangle$ given by Eq. (19). The "Numerical" model is a full numerical evaluation of the $I$ term in the scattering amplitude equations, without performing any Taylor approximations of the Green's function and using the original definition for G in Eq. (6).

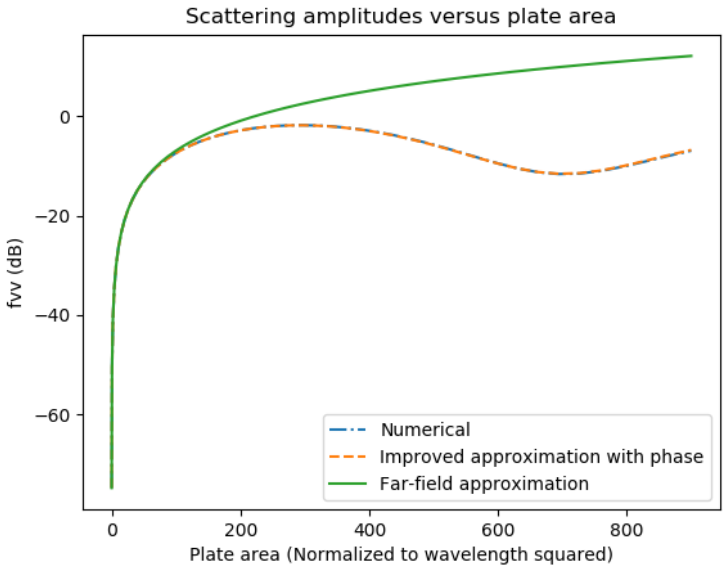


**Figure 7.** Scattering amplitude $f_{vv}$ (decibel scale) in the specular direction versus plate area $\frac{(2a)(2b)}{\lambda^2}$ for different Green's function evaluations, for a flat plate. $f_{vv}$ is evaluated at a distance $R_0 = 100\lambda$ from the center of the plate. The incident angle is (normal incidence).

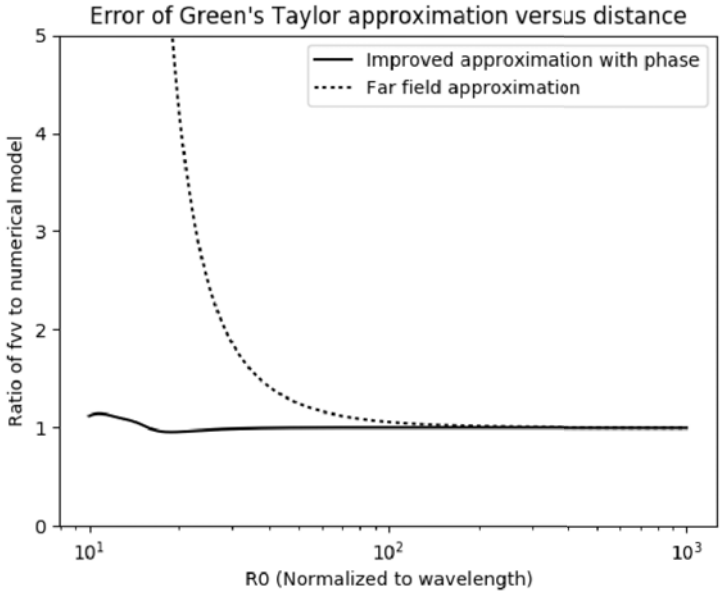


**Figure 8.** Ratio between $f_{vv}$ for our approximations and $f_{vv}$ from numerical evaluation in the specular direction, versus $R_0$ for a $10\lambda \times 10\lambda$ plate. The incident angle is (normal incidence).

As seen in Fig. 7, for small plate areas, agreement is very close. However, once the area exceeds about $150\lambda^2$, the far-field approximation is no longer a good model. The improved approximation is in close agreement with the full numerical evaluation. The error for our two Green's function approximations is visualized in Fig. 8.

Figure 8 better demonstrates the relative accuracy of the improved approximation for near field calculations. Very close agreement can be observed at $R_0 > 2\lambda$ for the improved approximation, as opposed to the far-field approximation which does not converge until $R_0 > 100\lambda$. For many practical

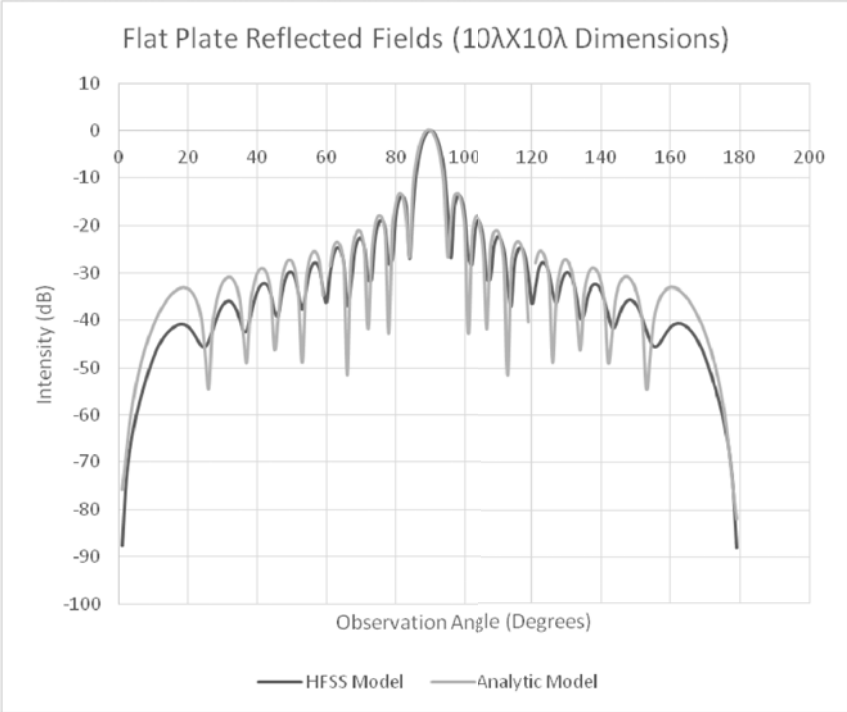


**Figure 9.** Comparison of numerical and analytic model. Plotting radiated fields $E_z$ for plate with $a = b = 5\lambda$, sweeping observation angle with normally incident wave.

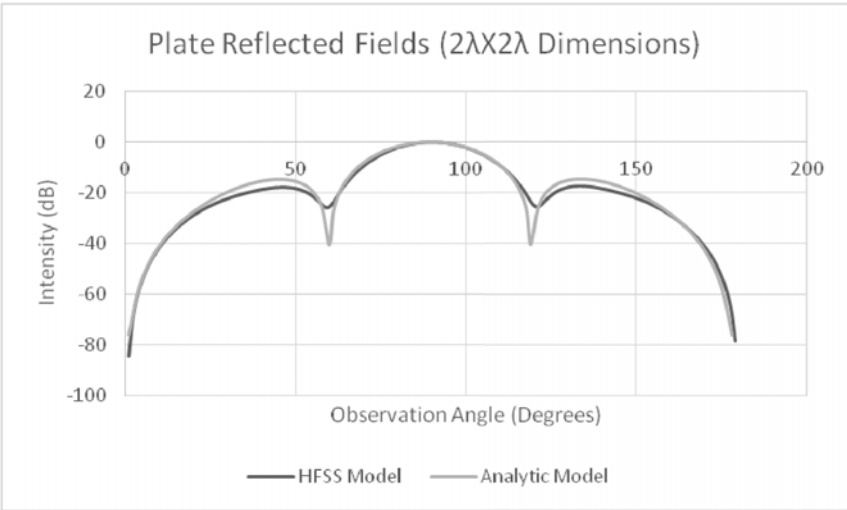


**Figure 10.** Comparison of numerical and analytic model. Plotting radiated fields $E_z$ for plate with $a = b = \lambda$, sweeping observation angle with normally incident wave.

situations, $R_0$ may not be much greater than the size of the plate including the case of low flying drones over an urban area.

### 4.2. Comparison with HFSS Data

Next, the equations were compared with numerical data. This is visualized in Figs. 9 and 10. In this case, a flat plate was used to speed up the numerical computation time. ANSYS HFSS was used for the numerical data, and the method derived in this paper was implemented in Python. A wave normally incident on the plate was considered, and the observation angle was modulated. Two different plate sizes were analyzed: $2\lambda \times 2\lambda$ and $10\lambda \times 10\lambda$. Very close agreement between the numerical and analytic models can be observed in the specular direction; however, as the observation direction approaches the edge of the plate, agreement starts to break down. The HFSS model includes plate edge effects, which are neglected in the analytic model. The agreement was relatively close for plates larger than $1\lambda \times 1\lambda$.

### 4.3. Multiple Plates

Next, multiple plate scattering was considered. Two situations were evaluated. One involved a transmitter at $\frac{\pi}{4}$ incidence on a $3 \times 3$ grid of uniformly spaced plates, all with the same orientation.

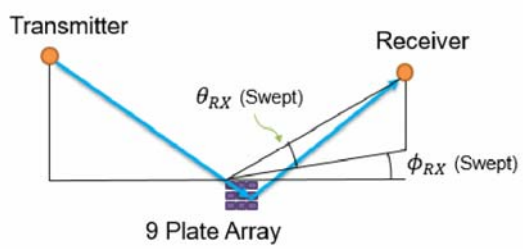


**Figure 11.** Locations of transmitter, receiver, and plates for data in Fig. 12.

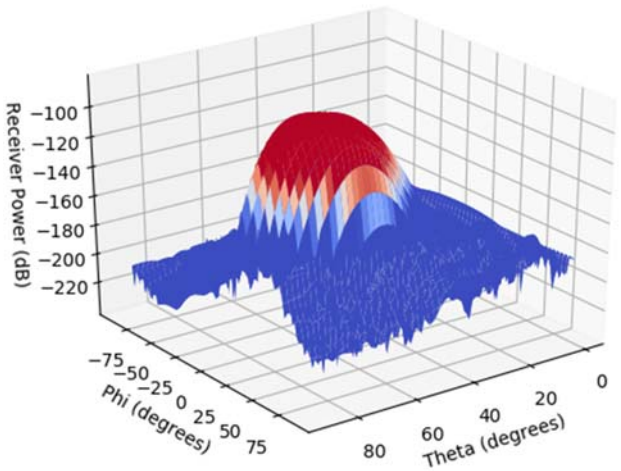


**Figure 12.** Receiver power versus observation angle for a $3 \times 3$ grid of plates, with a corner at the origin. The spacing between each plate on the grid is $12.5\lambda$. Frequency is 28 GHz. Transmitter and receiver are $100\lambda$ from origin, with transmitter at $\theta_i = \frac{\pi}{4}$, $\phi_i = 0$. Each plate is $5\lambda \times 5\lambda$, with $\langle h \rangle = 0.1\lambda$, $l = 3\lambda$, and permittivity $\epsilon_r = 7 + i0.35$.

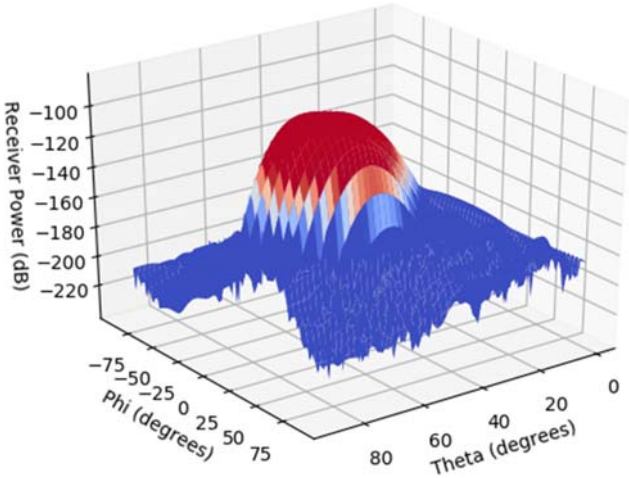


**Figure 13.** Receiver power versus observation angle for 10 randomly placed plates, centered at the origin. Each plate location is picked from a uniform random number distribution spanning $-66.67\lambda \leq x \leq 66.67\lambda$, $-75\lambda \leq y \leq 75\lambda$, $0 \leq z \leq 75\frac{\sqrt{2}}{2}$ Frequency is 28 GHz. Transmitter and receiver are $100\lambda$ from origin, with transmitter at $\theta_i = \frac{\pi}{4}$, $\phi_i = 0$. Each plate is $5\lambda \times 5\lambda$, with $\langle h \rangle = 0.1\lambda$, $l = 3\lambda$, and permittivity $\epsilon_r = 7 + i0.35$.

The second case was a transmitter at $\frac{\pi}{4}$ incidence on a distribution of 10 plates, each with a random position and orientation. Each simulation was run with the transmitter and receiver at distances $100\lambda$ from the origin. The setup is visualized in Fig. 11, and the results are visualized in Figs. 12 and 13.

The uniformly spaced plate array displays a clear peak in the specular direction from the array, with sinc-like falloff in the diffuse directions. The random plate distribution has multiple peaks, and in addition, one of the regions is inside the shadow of another plate.

## 5. CONCLUSION

This paper outlines a method for determining the radiation characteristic of a distribution of rough plates. Due to the use of analytic formulas, the method has a significant computational advantage over numerical methods. Several approximations were used to derive this formula that must be considered in practice. These include the neglecting of the edge effect and the modeling of an infinitely thick plate. In addition, all interactions using the formulas must be in the far field, and the area of a plate must be larger than $1\lambda \times 1\lambda$. Although the improved approximation of the Green's function is effective for the receiver close to the plate, the current formulation still assumes that the incident wave is a plane wave. The model can be improved using the spherical incident wave. Even given these approximations, this method is well suited for modeling scattering from geometry that can be represented as a set of planar structures with roughness. This method can be used to analyze behavior such as interference from reflections off of surfaces in urban environments, or radiation in areas such as solar panel arrays. Although this paper deals with a large thick rough plate, we have also studied the scattering from a thin dielectric plate which can be applied to leaves of deciduous trees [10].

## ACKNOWLEDGMENT

This work was supported by NSC-16-05-001.

## REFERENCES

1. Ruck, G., D. Barrick, W. Stuart, and C. Krichbaum, *Radar Cross Section Handbook*, 523–526, Plenum Press, New York, NY, 1970.
2. Johnson, J., R. T. Shin, J. A. Kong, L. Tsang, and K. Pak, "A numerical study of the composite surface model for ocean backscattering," *IEEE Trans. Geosci. Remote Sens.*, Vol. 36, No. 1, 72–83, 1998.
3. Li, Q., M. Y. Xia, L. Tsang, L. Zhou, C. H. Chan, and Z. X. Li, "Rough surface scattering: Numerical simulations and applications in microwave remote sensing," *Wiley Encyclopedia of RF and Microwave Engineering*, K. Chang (Ed.), 2005.
4. Desanto, J. A. and G. S. Brown, "Analytical techniques for multiple scattering from rough surfaces," *Progress in Optics*, Vol. XXIII, 1986.
5. Yueh, H. A., R. T. Shin, and J. A. Kong, "Scattering from randomly perturbed periodic and quasiperiodic surfaces," *Progress In Electromagnetics Research*, 1989.
6. Shramkov, O. I. and A. Y. Sukharevsky, "High-frequency method of antenna directional pattern calculation," *Journal of Electromagnetic Waves and Applications*, Vol. 21, No. 14, 2009–2023, 2007.
7. Ishimaru, A., C. Le, Y. Kuga, L. A. Sengers, and T. K. Chan, "Polarimetric scattering theory for high slope rough surfaces," *Progress In Electromagnetics Research*, Vol. 14, Nos. 1–36, 3–12, 1996.
8. Ishimaru, A., *Electromagnetic Wave Propagation, Radiation, and Scattering*, Vol. 2, 198–199, IEEE Press-Wiley, New York, NY, 2017.
9. Tsang, L., J. A. Kong, and R. T. Shin, *Theory of Microwave Remote Sensing*, Wiley-Interscience, New York, 1985.
10. Walborn, B., Y. Liu, M. Bright, A. Ishimaru, and Y. Kuga, "Modeling EM wave scattering from tree leaves," *URSI Meeting*, Boulder, 2018.